Results in Engineering 28 (2025) 107551

Contents lists available at ScienceDirect

Results in Engineering

journal homepage: www.sciencedirect.com/journal/results-in-engineering

Review article

Artificial intelligence supported semi-active suspension system design for motorcycles

Serkan Beller

Çukurova University, Vocational School of İmamoğlu, Natural Gas, and Fitting Technology Program, Adana, Turkey

ARTICLE INFO

Keywords:
Motorcycle
Semi-active suspension system
Artificial neural networks
CFBNN
GRNN

ABSTRACT

Shock absorber adjustment on motorcycles is critical for ride comfort, road holding, and safety. Correctly adjusted shock absorbers ensure that the motorcycle adapts optimally to the road conditions and make it easier for the rider to maintain control. Shock absorbers absorb the energy produced by the springs and the impacts they receive from the road and convert it into heat energy, which is transferred to the atmosphere and partly to the chassis. In addition to the flow rate of the oil passing through holes of varying sizes, the thickness of the oil also determines the movement speed of the shock absorber. The springs work in conjunction with the oil, and their stiffness is sensitive to the load and the location of the shocks. Damping adjustment is made via holes or valves and is sensitive to speed. A motorcycle with an incorrect shock absorber adjustment can be ridden, but if the spring stiffness is not appropriate for the rider's weight, riding will be impossible. In this study, a reservoir shock absorber was subjected to a dynamic test with different spring stiffness settings and CST (Kinematic viscosity, Centistokes mm^2/s) values of silicone oils. During the experiments, different weights were dropped onto the shock absorber from variable heights to simulate different dynamic driving conditions. Thus, the amounts and durations of shock absorber sag and springback were examined. With the artificial intelligence-based control block developed in the Simulink environment, different driving modes can be adjusted automatically or manually according to variable road conditions.

1. Introduction

The suspension system is a mechanism that ensures optimum contact of the wheels with the road surface, which directly affects the road holding and driving comfort of a vehicle. While the vehicle is in motion, bumps, potholes, and uneven ground on the road can be transmitted directly to the chassis and the driver via the wheels. The suspension system, consisting of shock absorbers, springs, and connecting elements, absorbs these impacts, increases the stability of the vehicle, and minimizes the shaking in the interior. If a vehicle does not have a good suspension system, vibrations, bouncing, and loss of road holding may occur [1].

A vehicle's suspension system is designed to increase driving safety and comfort by improving road holding. Ensuring that the wheels are in constant contact with the ground reduces the risk of skidding, especially on bends, and maintains stability during braking. Suspension components absorb impacts from the road surface, ensuring that less vibration is transmitted to the chassis and passengers. It also prevents irregular tire wear, thus extending tire life and optimizing fuel consumption. While stiffer suspension systems provide better road holding and performance, softer suspension systems offer a comfort-oriented ride. Car suspensions balance the vehicle's weight distribution, increasing load-carrying capacity and optimizing shock absorption [1].

A suspension system works like a launch mechanism. During operation, the shock absorber is forced to close when weight is applied to it. After the shock absorber starts to close, the shock absorber shaft tries to move downward in the cylinder filled with hydraulic oil. However, since liquids cannot be compressed, hydraulic fluid is displaced. As the piston continues to press, hydraulic fluid tries to escape from the end of the piston. Thus, most of the pressure on the shock absorber is counteracted by the friction force of the hydraulic fluid. When pressure is applied to the shock absorber in the opposite direction, the opposite happens. It doesn't matter whether it's expansion or compression. As a result, the movement of the piston in the shock absorber is slowed down and transmitted. Thus, the oscillation and vibration actions in the wheel are eliminated in a short time [2].

The springs on the shock absorber keep the body above ground level. The primary function of the spring is to return the stem to its preloaded

E-mail address: sbeller@cu.edu.tr.

https://doi.org/10.1016/j.rineng.2025.107551
Received 19 June 2025; Received in revised form 27 September 2025; Accepted 1 October 2025
Available online 2 October 2025
2590-1230/© 2025 The Author. Published by Elsevier B.V. This is an open access article under the CC BY-NC-ND license (http://creativecommons.org/licenses/by-nc-nd/4.0/).

set height after each compression or collapse of the stem. Springs are not the load-bearing elements in the suspension system. Ride height and collapse distance can be adjusted by inserting parts or by changing the spring itself, but other than that, the springs have no function in changing the load-carrying capacity of the suspension [3].

Hydraulics, that is, the fluids in the suspension, are not compressible like gases. The volume of the gas can be reduced by compressing it, but in this case, the gas turns into a liquid. Liquid volume cannot be reduced; that is, it cannot be compressed. The valves at the end of the shaft determine the flow rate of the oil and, therefore, the compression rate of the suspensions. If the valves are small, the movement will be slow; if large, the movement will be fast. This will allow the ascent and descent time to be slow or fast. This rule applies to both compression and rebound in both directions. Many modern motorcycle forks have adjuster knobs mounted on them to adjust these valves. Only the speed, namely the compression and rebound speed, is adjusted here [3].

When looking at previous studies, it was seen that two different fuzzy logic approaches were discussed in the article [4]. Here, the logic of the skyhook algorithm was basically taken into account. The disadvantage of these systems, the cost issue, was overcome by obtaining similar results with much fewer sensors. The results obtained in the simulation with fuzzy logic controllers were compared with the results obtained with the skyhook algorithm. It was observed that similar performances were obtained. Studies were carried out both in simulation and experimentally. In the study [5], a frequency division hybrid control algorithm (HCFD) was studied. The aim was to improve ride comfort and avoid the problem of road holding performance deterioration caused by traditional control algorithms (Skyhook…). Skyhook linear control was used to improve both ride comfort and road holding performance in the low and mid-frequency bands. In the high-frequency bands, hybrid control was used to suppress wheel resonance. The experimental results were compared with the classical control algorithm. The results showed that the vertical acceleration of the saddle position was effectively reduced, and the problem of road holding performance deterioration was prevented. Studies were carried out both in simulation and experimentally. In the study [6], the hardware in the loop (HiL) method was applied to develop a semi-active suspension system. This method is a testing method in which real-time measurements on physical hardware are used instead of a mathematical model of a particular hardware in the simulation. Thus, components without adequate models can be included in the simulation. The research explored whether a certain actuator-controller pair was suitable for conducting fatigue tests. HiL was also compared with a physical (Ballast-based) two-DOF system involving the rear suspension of a motorcycle. As a result of the tests, comparisons between HiL and software responses indicated that it is suitable for testing suspension systems. It was found to provide a viable alternative to ballast-based suspension tests by using existing equipment. Studies were carried out both in simulation and experimentally. In article [7], the semi-active suspension system was modeled using a quarter car model in the Simulink environment, too. Here, a fuzzy logic controller is modeled to modulate the damping coefficient value. Three semi-active suspension systems were simulated by modeling the road deterioration profile. The optimized system performed well by meeting the requirements of minimum percentage overshoot and fast balancing time. The studies were carried out in a simulation environment. In the article [8], the aim was to simulate and analyze the behavior of a motorcycle with semi-active suspension. The study dealt with the approach of LQR methodology to create a control system for semi-active vehicle suspension systems in both front and rear suspension of the motorcycle to promote comfort and ride. The MF tire was also taken into consideration to determine the efficiency of the motorcycle. The studies were carried out in a simulation environment. In the article [9], a study was conducted to make the semi-active suspension system control in motorcycles fault-tolerant. The proposed IFA scheme is based on the adoption of an NARX artificial neural network to realize suitable soft sensors. The work in [10] is a study on the optimum design of a soft displacement sensor that can be adapted to the rear suspension of two-wheeled vehicles. Experimental results show that the NARX model can provide a useful benchmark in implementing preliminary Instrument Failure Detection strategies for motorcycle rear stroke sensors. The study in [11] investigates the accuracy of a soft sensor used to estimate suspension speed in real time using acceleration signals. The second (Black box) approach, based on a Recurrent Neural Network, enabled the development of a soft sensor that can accurately estimate the suspension speed at lower ranges. In the article [12], it is intended to predict the velocity of extension in a motorcycle electro-hydraulic suspension is estimated with several accelerometers or a single sensor on the wheel side. Here, the Kalman filtering approach effectively solves the estimation problem by overcoming the vibration disturbances that greatly affect the accelerometers. In paper [13], a gray box model of a racing motorcycle monotube shock absorber was developed, which consists of a nonlinear parametric model and a neural network-based black box model. This model has shown significant improvement in force prediction ability over traditional linear models, nonlinear static velocity-dependent models, and models based solely on neural networks. Additionally, this parametric model can capture low-frequency macroscopic events. In article [14], a troubleshooting scheme for the motorcycle rear suspension stroke sensor is studied. In the study, it was seen that the NARX Neural Network trained with real data obtained in the field is a very reliable tool in estimating the expected value of the sensor output.

When the above studies were examined, it was seen that generally the studies were carried out as alternatives to the skyhook or to improve it. Apart from this, modeling and testing of semi-active suspension systems were also among the other researched topics.

1.1. Purpose of the study

In the study numbered [15], a quarter car model was studied and an examination was made based on suspended mass displacement and non-suspended mass displacement in accordance with the performance criteria. In this respect, sine signal and swept sine signal were applied as input to the models. For comparison in simulations, the existing passive suspension system parameters of the four-wheeled commercial test vehicle were used for the passive model. The developed control algorithms were compared with this passive model, and the resulting improvements were evaluated within this framework. In these simulations, the road displacement at frequencies of 1–20 Hz and 10 mm amplitude was entered into the quarter car model and at the end, four state variables of the quarter car model were examined. As seen in the studies, the improvement that the Skyhook controller creates for comfort has negative consequences for road holding. This is an example of how comfort and road holding properties are inversely proportional to each other. The c_{sa} magnitude used in the current simulation is taken as the maximum damping ratio. In simulations, the value of α is a measure of how much damping is distributed between the wheel and the body. The value α is a weighting coefficient in the linear Skyhook controller. This value was taken as 0.5 in the current simulations and the damper force was distributed equally to the suspended and non-suspended masses.

Since the semi-active suspension system works according to the relative speed between the body and the wheel, it is not as effective as active suspensions in active body control applications because it cannot provide sufficient force in places where this relative speed is low. In the tests performed, the semi-active suspension system is closest to the passive suspension since the relative speed in each quarter of the vehicle is low during the yawing motion. However, in maneuvers with high pitching motion, such as sudden braking, the relative speed increases, and therefore, body movements are controlled more effectively [15]. In other simulations performed in the CARMAKER environment, similar results were obtained as in the previous results [15]. While Skyhook is better in terms of comfort features, other algorithms are ahead in terms of road holding. The current study aims to improve the road-holding

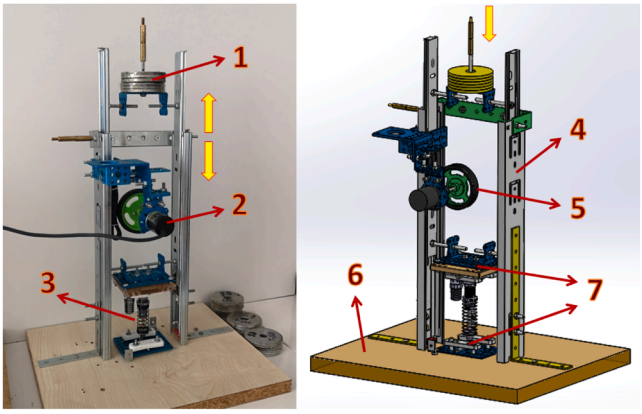


Fig. 1. Shock absorber experiment set: 1- Test weights, 2-Encoder, 3- Shock absorber with a reservoir, 4- Telescopic rail, 5- Robotic rubber-based wheel, 6-Chipboard floor, 7- Makeblock mechanical fittings.

properties of the shock absorber. Various methods can be applied to increase the roadholding properties of a shock absorber, such as improving the suspension system, checking the condition of the tires, and lowering the vehicle's center of gravity. Using sport springs, adjustable shock absorbers, or suspension kits to improve the suspension system can significantly increase road holding. Adjustable shock absorbers optimize roadholding by adjusting shock absorber firmness to suit different driving conditions. Here too, using artificial intelligence methods for road analysis will help the shock absorber make the most appropriate shock absorber stiffness settings according to different driving conditions.

1.2. Results obtained from the study

In the current study, the following results were obtained. In this study, while creating the model, real-time measurement values obtained from experimental studies were used instead of the mathematical model of the classical control algorithm, Skyhook. Thanks to the tests, the most suitable spring compression values according to the ideal driving mode results and the oil tank emptying speed according to different oil CST values and road structure were decided. Artificial intelligence methods were used to analyze current road conditions using nine different types of data. A high success rate was achieved in the artificial intelligence training and test data results. The existing control system can also be adapted to vehicles with more than two wheels. With a minimum number of sensors, the system can be easily adapted to any vehicle. Driving comfort will be increased thanks to the independent movement provided on each wheel in the vehicles.

In the second part of the article, the experimental set equipment was introduced, and spring and suspension sizing were performed. Additionally, the calculation of error values, the conduct of experiments, system design, and artificial intelligence methods are emphasized. In the third chapter, experimental studies and their results are discussed. In the fourth section, comparisons of experimental results were made, and the discussions of these results were presented in the fifth section.

2. Material and methods

2.1. Material

In this study, two telescopic rails 300 mm, Makeblock mechanical fittings, RC vehicle shock absorber with a reservoir (Tixiyu, 12 × 8 × 2, 90 mm aluminum alloy), Humusoft MF 634 DAQ card, Encoder Omron E6A2 CW3C, robotic rubber-based wheel (Θ 60 mm), and a computer (Windows 10, 64 bit, Intel Core i5, 3.40 GHz, 16 GB) were used as seen in Fig. 1.

2.1.1. Determination of suspension parameters

2.1.1.1. Suspension. The energy generated by impacts between the road bumps and the wheels should be as low as possible. Some of this energy is taken by shock absorbers and springs. The remaining energy must be transmitted to the suspended masses only at a frequency that can be easily tolerated. The term suspension refers to all elements placed between the passengers or cargo being carried and the ground. This term includes the wheels and chassis, which change shape with load and impact, along with springs, shock absorbers, tires, and seats. The suspension system works together with the chassis frame or unibody, wheels, wheel bearings, braking system, and steering system to provide a reliable and comfortable ride [16].

2.1.1.2. Semi-active suspension system. The semi-active suspension system is widely used among current motorcycle brands under the names BMW Dynamic Damping Control, Ducati Skyhook Suspension, and Marzocchi's Semi-Active System. The 2013 Ducati Multistrada with Ducati Skyhook Suspension (DSS) and the BMW HP4 with Dynamic Damping Control (DDC) are the first production motorcycles to feature semi-active suspension systems, a technology that has been commonplace in the automotive world for a long time. Truly active suspensions, like the Bose system, have no springs or shock absorbers. Instead, linear electromagnetic motors are used to directly control the wheel by literally lifting it over a bump or pushing it into a pothole. This ensures that the vehicle's body moves as steadily as possible [17].

The semi-active suspension system is a completely different system from active suspensions or electronically adjustable systems. In a fully-active system, electromagnetic or hydraulic structures completely replace the spring and shock absorber and "actively" control the position of the wheel relative to the chassis. The weight and complexity of these structures currently preclude the use of active suspension on motorcycles and make it seldom used in cars.

Electronically adjustable systems, such as BMW's ESA (Electronic Suspension Adjustment), Ducati's Electronic Suspension (DES), Öhlins Mechatronics, and the system used in the MV Agusta F4 RR are generally considered semi-active. This is true in some respects. These systems work by attaching small servo motors to the fork and shock adjusters. Servo motors vary in damping (And in some cases preload) depending on conditions or a mode selected by the driver. In practice, the slow response time of a tenth of a second severely limits their ability to adapt to general conditions in certain situations [17].In contrast to all this, a true semi-active system uses electronically controlled valves inside the fork or shock absorber, allowing damping changes to be made in milliseconds. This means the suspension is quick enough to adapt to every bump in the road. Standard springs are still used. What separates semi-active and fully-active systems is this: Active suspension systems can actively push the wheel down into a pothole or lift it over a bump, while semi-active systems depend on the road surface or springs to physically move the wheel [17].

2.1.1.3. Skyhook algorithm. In the semi-active suspension system, three basic control algorithms are used: Skyhook, Groundhook, and Hybrid controllers. Each algorithm allows for a change of the suspension characteristics of the vehicle by affecting the comfort or road holding [18].

The control system used in vehicles is a two-level structure. First, there is a lower-level control structure at the lower level, where each suspension can be controlled independently. Then, there is an upper-level control structure that can either change the control parameters according to the situation or temporarily replace the lower-level controls. In this context, while the lower-level control structures provide control in line with the movement of the vehicle's four suspensions, the upper-level control monitors the effects of the vehicle's vertical movement as well as head hitting and yawing movements. However, the

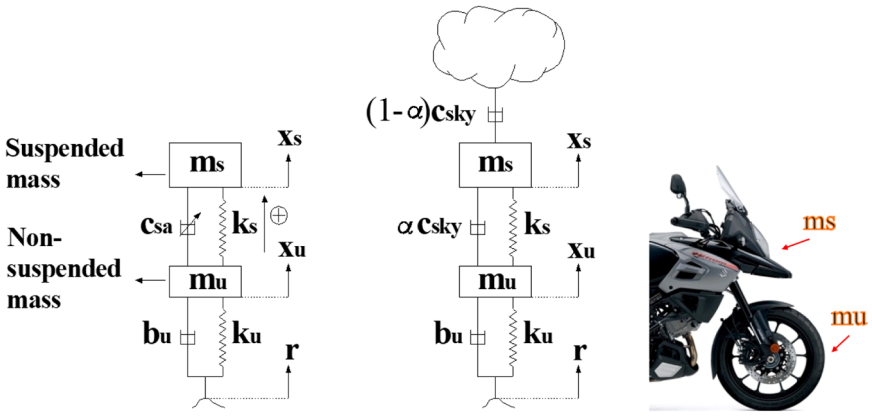


Fig. 2. Skyhook control algorithm: real and ideal cases.

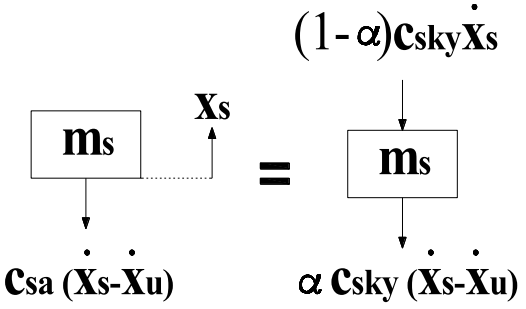


Fig. 3. Skyhook control algorithm: Damper forces.

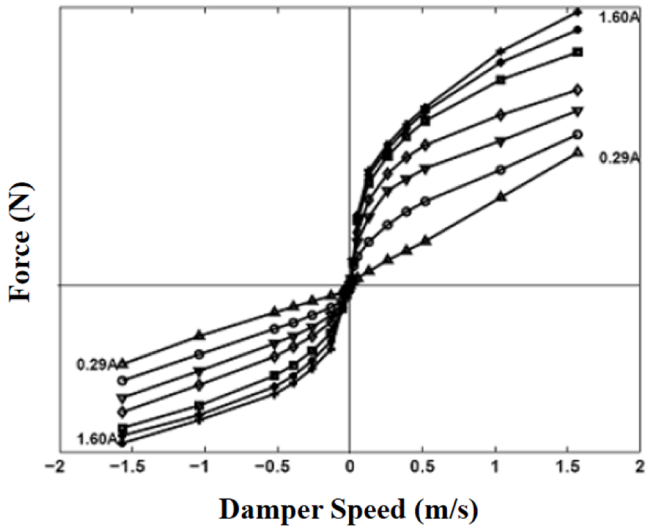


Fig. 4. Operating regions of the semi-active damper.

problem here is the situation that occurs when the head-hitting and pitching motions are assumed to occur simultaneously. For this purpose, the Transient Active Body Control (TABC) algorithm was designed, and its results were observed in simulations [15].

In the control algorithm Skyhook, which is used as a low-level control, the dampers try to create the effect of a virtual force. First of all, thanks to this control algorithm that controls each suspension independently, the stiffness of the suspension is changed in line with the wheel and body movements. The basis of these control algorithms is based on a control concept that aims to create a virtual damping effect. The second part of the control structure, the superstructure controller, monitors all suspension behaviors of the vehicle and controls body movements such as head hitting or yawing. For example, in order to prevent the vehicle from leaning to one side during the bend, the infrastructure controllers of the side suspension system are disabled during the turn, and the suspensions here are stiffened to prevent unwanted movement [15].

As a result of the control structure taking a hierarchical form, performance criteria can be expanded by going through the full vehicle model. The controller's task is no longer limited to controlling only vertical movements, but also intervenes in unwanted pitching and rolling movements of the vehicle. In fact, changing the damping ratio does not change the static equilibrium position. For example, let's assume that the head hitting movement during braking occurs with a static moment. A passive suspension model with the same spring coefficient and a semi-active suspension system will reach the same equilibrium point in a steady state, and as a result, the same head hitting angle will occur. However, increasing the damping ratio will reduce the overshoot that occurs in the passive suspension. Considering that both the braking and yawing movements do not last long enough to reach a steady state, it has been proven in simulations that a semi-active suspension system will significantly reduce these movements [15].

While Ducati includes the term 'Skyhook' in its definition of DSS, the term in fact describes a widely used approach to semi-active suspension control [17]. As represented in Fig. 2, the general structure of the Skyhook control is shown. The ideal situation on the right is attempted to be created with the real suspension structure with the semi-active damper added on the left. In the ideal structure on the right, the suspended mass of the motorcycle is connected to a fixed point with a virtual damper, and thus the motion of the suspended mass is tried to be damped by two dampers. The movement of the body, which is also attached to a fixed point, will give better results than the situation where it is attached only to the wheels. However, since such a connection is not possible, the same effect is approached with a semi-active suspension system [15].

In Fig. 3, only the effect of the damper forces on the masses is seen in the ideal and real cases. On the left side, the force that can be obtained with the real damper is shown, and on the right side, the forces generated by the ideal situation are shown. If these two forces are equalized, the force required to be created in the actual damper is obtained [15].

Mathematically speaking, the damper forces on a mass attached to a fixed point can be expressed with the following equations.

$$F_{damper} = -(1-\alpha)c_{sky}\dot{x}_s - \alpha c_{sky}\left(\dot{x}_s - \dot{x}_u\right) = -c_{sa}\left(\dot{x}_s - \dot{x}_u\right) \quad (1)$$

$$c_{sa} = \frac{(1-\alpha)c_{sky}\dot{x}_s + \alpha c_{sky}\left(\dot{x}_s - \dot{x}_u\right)}{\left(\dot{x}_s - \dot{x}_u\right)} \tag{2}$$

Thus, the ideal state configuration of the semi-active suspension coefficient obtained in Eq. (2) is provided [15]. However, since semi-active dampers cannot create force in the same direction as the movement, that is, they are only a friction or damping element, there are some conditions for the equation obtained above [15].

As is known, the damper operates only in the second and third regions of the graph shown in Fig. 4. It cannot produce a negative force in tension or a positive force in compression. In other words, there are no force effects in the first and fourth quadrants. Knowing these operating conditions will be useful in understanding the threshold values that complement the Skyhook control equations [15].

Accordingly,

$$\dot{x}_s(\dot{x}_s - \dot{x}_u) \geq 0 \Rightarrow c_{sa} \tag{3}$$

$$\dot{x}_s(\dot{x}_s - \dot{x}_u) \leq 0 \Rightarrow c_{min} \tag{4}$$

By creating the above conditions, Skyhook control is made suitable for the situations in which semi-active dampers can operate. Accordingly, when condition (1) is valid, the c_{sa} damping coefficient calculated in the above equations is used, while when condition (2) is valid, the smallest damping coefficient that the damper can provide is used. The reason for this can be revealed by examining the different situations that these conditions create. As can be seen, due to the structure of the semi-active damper, the completely ideal Skyhook model can not be achieved. This can only be achieved in the presence of an active damper capable of generating force. As seen in Fig. 2, the Skyhook model connects the body with two different dampers, both to a fixed point and to the wheel mass. In some ideal Skyhook models found in the literature, this second damper between the body and the damper is not used and only body oscillations are taken into account. However, in the linear Skyhook model that is desired to be approached with the controller used, the wheel movements are also under control. Thanks to the α factor, in the ideal case, the damping force acts on both the wheels and the body. This means that not only body movement but also wheel forces are taken into account. When the ideal situation is approached, this effect is also created with the damping coefficient c_{sa}. The α coefficient is actually a coefficient that provides the transition between comfort and road holding [15].

2.1.1.4. Skyhook algorithm analysis. The vehicle models used in developing the semi-active suspension model are the quarter-car model, the half-car model, and the full-car model. However, it should be noted that the goal here is not to create a model that accurately reflects the suspension system, but rather to create a model sufficient for controller design. The quarter-car model is an adequate model for these features, as seen in both the literature and the current study [15].

The control system used in vehicles has a two-level structure. First, there is a lower-level control system that can control each suspension independently, followed by a higher-level control system that can either change control parameters as needed or temporarily replace the lower-level controls. The lower-level control systems create a control system that aligns with the motion of the vehicle's four suspensions. The upper-level control system addresses the effects of the vehicle's vertical motion, as well as pitching and yawing [15].

The control algorithm used as the lower-level control within the control structure is the Skyhook. This structure is widely used in practice. In this structure, the dampers attempt to create the effect of a virtual force. This control algorithm, which controls each suspension independently, modifies the suspension's stiffness based on wheel and body movements. These control algorithms are based on a control approach that aims to create a virtual damping effect.

The second part of the control system, the superstructure controller, monitors all vehicle suspension behaviors and controls body movements such as head-on or pitching. For example, to prevent the vehicle from leaning to one side during a corner, the substructure controllers for the side suspension system are disabled during the turn. This stiffens the suspensions there to prevent undesirable movement.

By taking this hierarchical control structure, performance criteria can be expanded by utilizing the full vehicle model. The controller's role is no longer limited to controlling vertical movements; it also intervenes in undesirable pitching and rolling movements of the vehicle. Changing the damping ratio does not actually change the static equilibrium position. For example, if it is assumed that the head-on movement during braking occurs with a static moment, a passive suspension model with the same spring coefficient and a semi-active suspension system will reach the same equilibrium point in the steady state, and the same head-on angle will occur as a result. However, increasing the damping ratio will reduce the overshoot that occurs in the passive suspension. Simulations have also demonstrated that a semi-active suspension system can significantly reduce these motions, assuming that neither the braking nor the pitching motions lasts long enough to reach a steady-state operation [15].

2.1.1.5. Shock absorbers. When a spring is compressed and released, it continues to shorten and lengthen for a while. These oscillations produce a very jerky and uncomfortable ride. If new pulses occur before the spring returns to its equilibrium position, the oscillations combine, and the amplitudes can reach dangerous values. An oscillating wheel is also dangerous in terms of safety, as it makes vehicle control difficult. Shock absorbers are used to dampen these oscillations. The function of single and double-tube shock absorbers is to quickly dampen the spring by restricting its oscillatory movements. The greater the acceleration given to the chassis (The more severe the impact), the stronger the damping must be. For this purpose, hydraulic shock absorbers are often used, in which damping is provided by the passage of a liquid (oil) from one place to another through small holes. These elements generally have little effect on the compression of the spring, but delay its opening [16].

The shock absorber is used in parallel with the suspension springs. In both single and twin tube shock absorbers, the master cylinder is divided into two chambers by a piston with holes and valves that restrict it and produce a damping force. In practice, pressurized nitrogen gas is often used to prevent potential cavitation of oil flowing at high speeds through small holes [16].

Low-pressure twin-tube shock absorbers have been used with some improvements since the 1960s. This design has features such as smooth valve movements and being more economical to produce than single-tube or adjustable types. Monotube high-pressure shock absorbers are a more modern application and run cooler. Hydraulic oil and nitrogen are separated into separate chambers by a floating piston. Thus, the shock absorber works without aeration and foaming. Monotube high-pressure shock absorbers have the ability to cope with greater impacts and have high damping ability. Most race cars use a single-tube design [16].

2.1.1.6. Shock absorbers with a reservoir. A reservoir is an integral part of the damping component. It significantly increases the oil volume in the damping circuit of the shock absorber. This capacitive expansion, with a larger surface area, has an immediate positive impact on the system's thermal performance. Both the increased oil volume and the expanded surface area of the reservoir act as a buffer against heat, allowing the shock absorber to dissipate and regulate heat more efficiently [19]. Shock absorbers with reservoirs generate less heat during off-road descents, maintain consistent performance even on long descents, and enhance control when following the same line with a consistent performance. Shock absorbers work overtime during off-road descents. Every bump, every fall, the shock absorbers absorb all the

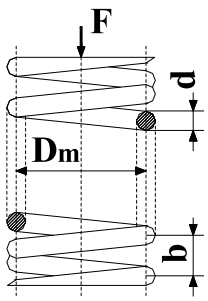


Fig. 5. Coil spring.

movement and convert it into a tremendous amount of kinetic energy. The closer these bumps are together, the greater the friction from the compression and rebound cycles, generating heat in the shock absorber's circulating oil. As the oil temperature increases, its viscosity changes; that is, it becomes thinner. The thicker the oil, the worse the damping performance. As the oil warms up, it means that finely tuned compression and rebound damping quickly lose their performance. This also adversely affects land performance [19].

An uncontrolled kickback is a potential safety hazard. The rear suspension no longer behaves as it should when two things happen: at full speed on a descent route, and when the suspension system becomes less effective due to temperature problems. If the shock absorber rebounds and compresses without proper damping, the risk of losing control during a descent increases significantly. One of the most dangerous events is when the rear of the bicycle starts to "kick". For example, the bicycle is approaching a jump point, ready to take off, and the shock absorber is already overheated. With rebound performance already degraded, when skidding off the edge of a jump, the rear end pushes the rider forward with a burst of unwanted power. This makes the landing front-weighted. This not only results in a loss of velocity but also a loss of control over the bike [19].

The thermal stability provided by a reservoir is extremely important. The reservoir keeps the shock absorber cooler and prevents the oil from foaming. This foaming is known as cavitation, a phenomenon that can compromise damping efficiency. When the oil temperature reaches 200 °C, it causes the oil to expand and lose its shock absorber characteristics. Shock absorbers with a reservoir contain more oil, so the time it takes to reach high temperatures may be longer. Another advantage of the shock absorber with a reservoir is that the cylinder is filled with oil. Normal shock absorbers contain a mixture of nitrogen and oil. As the shaft of the shock absorber enters the cylinder, the oil moves into the reservoir. This is what makes the difference. This results in much higher performance and driving quality. Another advantage of the shock absorber with a reservoir is that there are no problems, such as cracking or bursting, during use. They do not have a structure that requires regular changes in normal or land use. Also, in shock absorbers without a reservoir, after the shock absorber loses its function, the vehicle starts to take impacts, depending on the terrain during the race. This causes the vehicle to break down and incur the cost of spare parts. As a result, thanks to shock absorbers with a reservoir, the shock absorber life increases, there is no need for constant replacement, the vehicle is less damaged, and better performance is achieved. Thus, thanks to these advantages, despite the high initial investment cost, the benefits it provides can tolerate it [20].

Shock absorbers with a reservoir are divided into two groups, Piggyback or Remote Reservoir, depending on the connection type of the reservoir tank to the shock absorber tube. In Piggybacks, the shock absorber tube and reservoir tank are produced as a single piece. They are extremely close to each other. Their performance is better than other types. They provide high precision in rough terrain landings [19]. However, not every vehicle may have enough space to use this type of shock absorber. In the Remote Reservoir system, the reservoir tank is connected to the main tube with a hydraulic hose. These types are preferred more in vehicles with space problems. In the present study, the Piggyback shock absorber type was preferred [20].

2.1.1.7. Springs. The vehicle body or chassis frame carries the weight of the engine, powertrain, passengers, and/or cargo. The body and chassis frame are supported by springs at each wheel. The weight of the chassis frame, body, and their attached members applies an initial compression to the springs. When the vehicle's wheels hit bumps in the road or fall into potholes, the springs are compressed further. Springs can not completely absorb road impacts. Some of the road irregularities are also absorbed by the tires. The springs in vehicle seats also help to cushion the impact to some extent. Three types of springs are generally used in suspension systems. These are bending springs, torsion springs, and air springs. In the current study, a study was conducted with a coil spring, which is a type of torsion spring [16].

An ideal vehicle suspension spring should absorb the shock quickly and then slowly return to its normal position. This is extremely hard to achieve. A spring that is too soft or flexible will have too much movement, while a spring that is too rigid or hard will give a ride that is too rough. To provide satisfactory ride quality, a medium-stiff spring and a shock absorber must be used together [16].

2.1.1.8. Coil springs. The coil spring is manufactured by winding the spring steel in bar form in a helical manner. They are cheap to manufacture and are the most widely used spring type. This type of spring is more flexible than a leaf spring and responds more smoothly to road irregularities. Coil springs do not generate friction, so a shock absorber is required to control the resulting oscillations. Due to their design features, coil springs can not be used against torque reaction or lateral loads. Therefore, to maintain proper geometry between the body and the suspension system, control arms and stabilizers are required [16].

2.1.1.9. Sizing suspension springs. In Fig. 5, F is the spring load (N), D_m is the average winding diameter (mm), n is the number of turns, G is the shear modulus (≈ 78500 N/mm^2 for hot-formed springs, ≈ 81400 N/mm^2 for cold-formed springs), d is the wire diameter (mm), and b is the space between turns (mm).

When the spring is under load F, the amount of deflection of the spring is,

$$s = \frac{8FD_m^3 n}{Gd^4} \tag{5}$$

torsional stress,

$$\tau_t = \frac{8FD_m}{\pi d^3} \tag{6}$$

wire diameter,

$$d = \sqrt[3]{\frac{8FD_m}{\pi\tau}} \tag{7}$$

number of turns,

$$n = \frac{sGd^4}{8FD_m^3} \tag{8}$$

length under load,

$$L_1 = n.d + n.b \tag{9}$$

free length,

$$L = L_1 + F.e = L_1 + s \tag{10}$$

and deflection under maximum load,

$$s = \frac{F}{2}.e \tag{11}$$

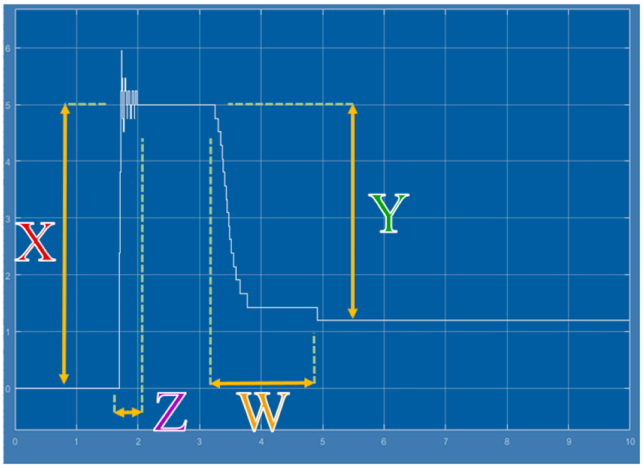


Fig. 6. Shock absorber movements under load: X: Descent amount (mm), Y: Springback amount (mm), Z: Descent time (s), W: Springback time (s), (Sample time: 0.01 s), (266 g-25 mm-5 mm-200 CST).

where e is elasticity(mm/N).

2.1.1.10. Suspension parameters. When a spring, loaded or unloaded, is suddenly compressed or expanded, it oscillates before returning to its equilibrium position. Period is the time it takes for one complete oscillation.

$$\tau = \frac{2\pi}{\omega} = 2\pi\sqrt{\frac{F_0 e}{g}} = 2\pi\sqrt{\frac{s_0}{g}} \tag{12}$$

Here, F_0 is the static force (N), s_0 is the static deflection (m), e is the elasticity (mm /N), and g is the acceleration due to gravity (9.81 m /s^2).

Since the frequencies that the human body can most easily tolerate are 65…80 oscillations per minute,

$$\tau = 0,75 - 0,9.s \tag{13}$$

static deflection of springs,

$$s_0 = \left(\frac{\tau}{2}\right)^2 \tag{14}$$

It should be at the level of 0.12 m … 0.20 m.

The elasticity of a suspension spring must be matched to the load it will carry. A spring that bends transfers a load to the chassis, and with this effect, the chassis rises. Everything around the wheels is unsprung mass and includes the wheels, axles, springs, brake discs, calipers, etc. Everything above the spring is also a sprung mass and includes the rest of the vehicle. If the mass of the unsprung members is m_{us}, the mass of the sprung members is m_s, and the vertical velocities of the wheel and chassis as a result of an impact are $\dot{z}_{us}$, $\dot{z}_s$, respectively, then from the amount of motion theorem,

$$m_{us}.\dot{z}_{us} = m_s.\dot{z}_s \tag{15}$$

can be written. In this case, as the $\frac{m_{us}}{m_s}$ ratio decreases, the $\dot{z}_s$ speed transmitted to the chassis decreases.

Reducing the weight of unsprung mass is very beneficial for handling, as the suspension system can control the wheels more easily. In terms of vehicle dynamics, reducing 1 kg of unsprung mass has the same impact as reducing 8 kg of sprung mass. Unsprung mass accounts for a significant portion of the vehicle's total mass. In standard vehicles, the ratio of these masses to each other is 13–15 %. Since the unsprung mass interacts directly with irregularities in the road, it creates significant vertical acceleration forces, especially at high highway speeds, reducing handling quality. As a result, in terms of damping of road impacts and comfort, the smaller the unsprung mass and the larger the sprung mass in a vehicle's suspension, the better [16].

2.1.2. Calculation of error values

Performance evaluations of training and test results were realized with Root Mean Square Error (RMSE), Regression Coefficient (R^2), and Mean Absolute Error (MAE) values. They were determined in Excel with the help of Eqs. (17), 18, and 19, respectively.

A_j = Actual values, P_j = Predicted values, n = Size of the data set, e_j =Error

$$e_j = A_j - P_j \tag{16}$$

Root Mean Square Error (RMSE), best value = 0, worst value = +∞

$$RMSE = \sqrt{\frac{1}{n}\sum_{t=1}^{n} e_j^2} \tag{17}$$

Regression Coefficient (R^2), best value = +1, worst value = -∞

TSS = Total Sum of Squares, RSS = Residual Sum of Squares

$$R^2 = \frac{TSS - RSS}{TSS} \tag{18}$$

Mean Absolute Error (MAE), best value = 0, worst value = +∞

$$MAE = \frac{1}{n}\sum_{t=1}^{n} |e_j| \tag{19}$$

Mean Squared Error (MSE) represents the average of the squared differences between actual and predicted values, reflecting the variance of the residuals. Root Mean Squared Error (RMSE), as the square root of MSE, indicates the standard deviation of the residuals. The measure of the agreement between the true value and the model's prediction is R^2. It is found by dividing the actual values' variance by the estimated values' variance. This situation expresses how good or not the model fits. Mean Absolute Error (MAE) represents the average of the absolute differences between predicted and actual values. It reflects the average size of the residuals in the dataset.

2.2. Methods

During the experimental studies, loads of different weights were dropped onto the shock absorber from different heights in free fall. The tests were run for 10 s simulation periods. Each test weight was allowed to remain on the shock absorber for 1–1.5 s. The test weights were then removed from the upper part of the shock absorber, where they had fallen. The graphical results of the data received from the encoder during the experiments were recorded. The data obtained from these graphs was used as training and test data in artificial intelligence methods. Fig. 6 represents an example of the graphs drawn by the encoder. The distance indicated by X indicates the amount of collapse in the shock absorber in mm when the test weight is dropped onto the shock absorber in free fall (Including the test set weight (225 g)). Y distance indicates the springback distance in millimeters when the test weight is removed from the shock absorber. The Z distance indicates the time until the shock absorber reaches its most stable state after the test weight is placed on it. The distance W indicates the time it takes for the shock absorber to reach its most stable state after the test weight is removed. Thus, a situation was made to simulate what occurs in the shock absorbers when the motorcycle enters a pothole, jumps from a high place (off-road), rides on asphalt, or does light off-roading.

During the experiments, it was not possible to achieve higher loads and higher heights. This is because the amplitude and frequency of the waves generated after the load first hits the ground increase. This creates the risk of the simulation ending within the W distance shown in Fig. 6 within the ten seconds experimental period. Therefore, achieving a

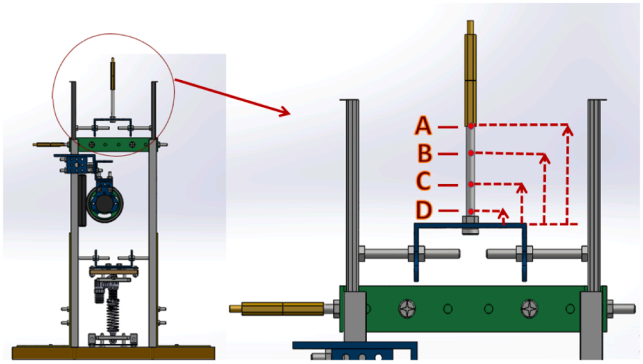


Fig. 7. Test weight points: A (35 mm), and D (1 mm) weight points for training, B (25 mm), and C (10 mm) weight points for testing.

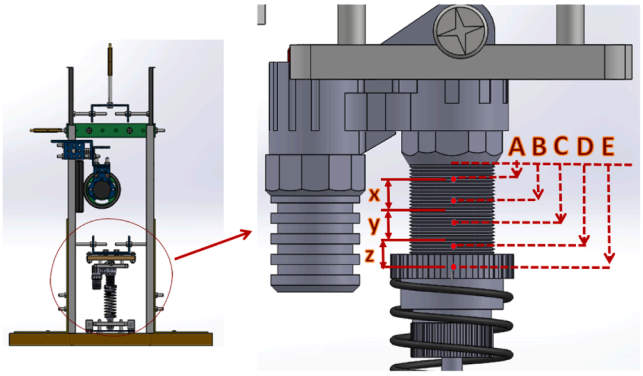


Fig. 8. Spring compression values: A: 1.5 mm, C: 9 mm, E: 16 mm for training data, B: 5 mm, D: 12 mm for test data. Shock absorber spring compression ranges: x: 1.5 mm… 6333 mm (For soft driving in off-road conditions), y: 6334 mm… 11,166 mm (For medium driving in light off-road conditions), z: 11,167 mm… 16 mm (For hard driving in asphalt conditions).

reliable Y distance can be difficult. Furthermore, the stability of the generated signal for at least one second can vary from time to time. The shock absorber stroke is 26 mm. The maximum deflection achieved in the training data is 14.272 mm. The maximum deflection achieved in the test data is 8.325 mm.

Different weights were used during the tests. 10 different weights were used for the training data. These are, respectively, 118 g, 136 g, 150 g, 179 g, 194 g, 254 g, 286 g, 315 g, 373 g, 400 g. For the test data, 9 different weights were used. These are, respectively, 125 g, 141 g, 166 g, 186 g, 225 g, 266 g, 307 g, 352 g, 391 g. All these weights were dropped onto the experimental set weight bed from different heights, as seen in Fig. 7. For the training data, these heights were determined as 1 mm and 35 mm, respectively, while for the test data, they were determined as 10 mm and 25 mm, respectively. Meanwhile, the standard test set weight on the test set shock absorber was measured as 225 g.

During the experiments, while the test weight amounts and free fall heights were changed, some changes were also made to the shock absorber. One of these is to change the amount of compression of the existing spring, and the other is to perform tests using shock absorber synthetic oils with different CST values. As seen in Fig. 8, the compression values of the current spring were determined as 1.5 mm, 9 mm, and 16 mm for the training data, while 5 mm and 12 mm were preferred for the test data. For synthetic oil, three different oils were used for training data. These oils are referred to by their viscosity values, which are indicated by CST (Centistokes, mm^2/s, 40 °C). The first of these was tests with zero CST, meaning no oil was added to the shock absorber (CST = 0). The CST values of the other two oils were preferred as 350 and 1000. For the test data, two different oil structures were used. Their CST values were determined as 200 and 500. Thus, shock absorber structures with different properties under different conditions were examined.

The shock absorber used in the current experimental set is one used in 1/10th scale RC vehicles. Silicone oils are the preferred oil for RC car shock absorbers. These oils have shock absorber oil values ranging from 0.65 to 1000 CST. For 1/10th scale electric on-road cars, an average CST range of 300–500 is preferred [21]. The types of oil used in motorcycles are mineral oils, fully synthetic oils, and semi-synthetic oils [22]. The CST values of these oils vary between 6 and 103 CST values [23,24]. Shock absorber oils have different viscosity values. They are generally classified as 2.5 W, 5 W, 10 W, 15 W, and 20 W. For softer suspension and a lighter ride feel, low-viscosity oils (2.5 W - 5 W) are preferred. For balanced damping, medium-viscosity oils (10 W - 15 W), and for stiffer suspension and sportier or heavily loaded motorcycles, high-viscosity oils (20 W and above) are preferred [25]. In the current test set, silicone oil CST values corresponding to the W values of oils suitable for various terrain conditions were selected.

As the CST value increases, the density of the shock absorber oil increases proportionally. The more fluid the oil (The lower the CST value), the less resistance the suspension piston will experience, resulting in faster response. However, when the oil is less fluid (The higher CST value), the suspension response is slower. For example, using an oil with a lower CST ratio on a Bumpy track with low grip allows the suspension to work faster, thus ensuring that the tires do not lose their grip on the road. However, if racing on a smooth track with good grip, the load on the suspension will increase, requiring a thicker oil for a stable ride [21]. In the current study, silicone oils with CST values of 0 and 200 were chosen for a smooth ride, CST values of 350 and 500 for a balanced ride, and CST values of 1000 for a sportier, harsher ride, too. Thus, when creating the training data, a main framework was created that included soft, medium, and hard rides (0, 350, and 1000 CST). Tests were conducted for soft and medium rides (200 and 500 CST).

Additionally, two different artificial intelligence methods from machine learning were preferred in this study. One of them is CFBNN, and the other is GRNN. In the CFBNN network structure, the training function is: trainbf, data division is: random, the number of input data is: 9, the number of output data is: 1, the number of neurons in the hidden layer is: 5, and the epoch value is: 1000. As seen in Fig. 9, the number of data inputs in the serially connected GRNN is 1, the number of data outputs is 1, and the number of neurons in the hidden layer is 180. Training was performed with different *spread* values in GRNN. As shown in Fig. 9, these two network structures were used in series connection. The first network (CFBNN) had training and testing success rates of 6.11 % and 5.56 % for a 5 % error, respectively. The serially connected GRNN network increased these success rates to 100 % in training and 98.96 % in testing with 5 % error. As can be seen in the picture, the results from the first network have at least twelve digits after the decimal point. These numbers cause each result to be different from the other. The GRNN network recognizes each digit as a different number, even if the integer parts are the same, because the digits after the decimal point are different. Therefore, it assigns a separate neuron to each value in the hidden layer during training. Thus, the success rate can be increased with serial usage [26,27].

2.2.1. System design

When looking at Fig. 10, a total of nine data types are seen as input data. These are, respectively, 1- Weight Value of Experiment Set (g), 2- Weight Value of Payload (g), 3- Height Value of Payload (mm), 4- Spring Compression Amount (x) (mm), 5- CST Value of Oil, 6- Shock Absorber Descent Amount (mm), 7- Shock Absorber Springback Amount (mm), 8- Shock Absorber Descent Time (s), and 9- Shock Absorber Springback Time (s). Here, data number one represents the motorcycle weight. Data number two shows the rider's weight, and data number three shows the free-fall height of the rider over the motorcycle seat when the motorcycle enters the pit. How much the shock absorber springs are

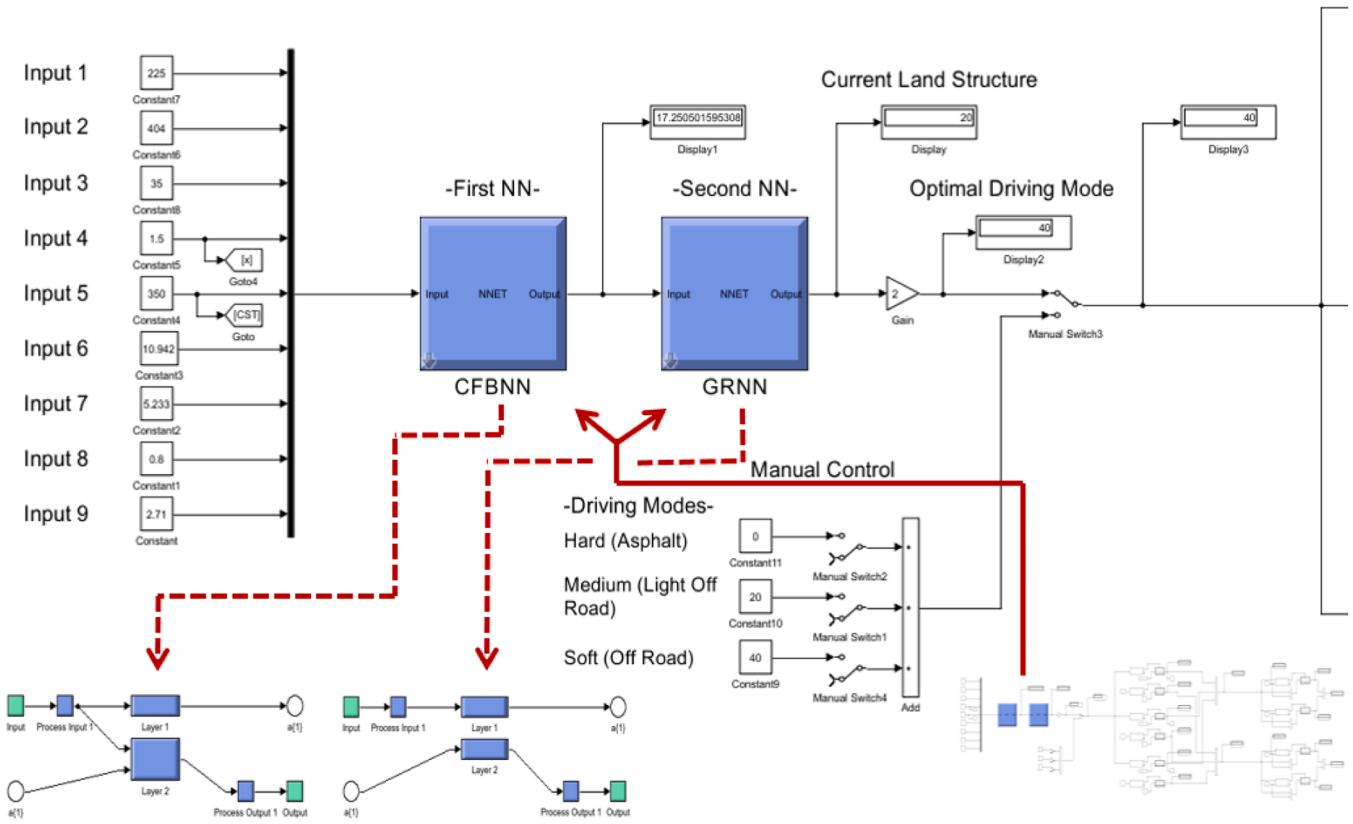


Fig. 9. Serial use of artificial intelligence methods.

compressed is shown by the fourth data point. It is similar to adjusting the automatic preload on motorcycles. (The method envisaged for this is either to use mini electric motors or to adapt the electro-hydraulic system.) The primary purpose of this control block is to adjust the stiffness settings of the shock absorber springs automatically or manually, depending on the current road structure. In terms of adaptation to off-road terrain, not only the spring but also the oil inside the shock absorber is quickly discharged into the reserve tank, ensuring that the shock absorbers operate more smoothly and are made suitable for the terrain. (In rally cars, long springs and soft shock absorbers are used. The grip is weak. Therefore, weight transfer is also tried to be used. More weight means more grip.) The method envisaged for this to happen is as follows. The diameter of the oil passage channel to the reserve tank will be automatically enlarged (This is a method used today. It is done with the Bump/Rebound settings.), and the oil will be discharged quickly from the main shock absorber tube. (Nowadays, nitrogen gas with a traveling piston or a spring mechanism is used to quickly drain the oil in the reserve tank back into the main tube [20]). Since the diameter of the transition channel to the reserve tank of the shock absorber used in the current experimental set is fixed, the oil in the shock absorber will be discharged quickly when the result shows minus (–) CST values in the Output 2 results in Fig. 10. On asphalt and light off-road terrain, only the spring stiffness settings are changed for soft, medium, and hard driving. There is no intervention in the current CST value or discharge rate of the oil. The CST value of the current oil used in the shock absorber is written in the fifth data.

The sixth data is how much the shock absorber descends under load, and the seventh is how much this springback is in millimeters. The eighth and ninth data include the descent time and springback time values, too. The second section of the system control block contains the Intelligent Controller section. Here, it is seen that CFBNN and GRNN networks are used in series. The aim of this section is to make decisions about the current road structure using nine types of input data. Whether the current road structure is asphalt, light terrain, or off-road, the information is shown by producing one of the numbers 0 (Asphalt), 10 (Light Off-Road), and 20 (Off-Road). The current road information data output from the intelligent controller group is then multiplied by the number two. Thus, a new type of data called Optimum Driving Mode (ODM) appears. There are two methods for obtaining ODM. It is either determined automatically according to the current road conditions with the intelligent controller block, or the driver determines it according to her/his wishes with the manual control block. In ODM, 0 represents hard driving, 20 represents medium driving, and 40 represents soft driving. Hard driving mode is suitable for asphalt driving. While the CST value of the shock absorber oil does not change, the spring compression value is brought to 13.583 mm (The hardest and most suitable average value. It is the midpoint of the z range in Fig. 8.). Medium driving mode is suitable for light off-road driving. While the CST value of the shock absorber oil does not change, the spring compression value is brought to 8.750 mm (The most moderate hardness and the most suitable average value. It is the midpoint of the y range in Fig. 8.). The soft driving mode is suitable for off-road driving. While the CST value of the shock absorber oil is brought to the zero position (Rapid discharge of the oil into the reserve tank.), the spring compression value is also brought to the value of 3.916 mm (The softest and most suitable average value. It is the midpoint of the x range in Fig. 8.). All of this is done with the if blocks under the main section, The Ideal Spring Compression Amount and Oil CST Value. Thus, the ideal spring compression value and the oil's CST value (Rapid discharge starting time of main tube) are found according to the current road conditions. In the last section of the system control block (Output 1), the differences between the current spring compression values and the ideal spring compression value are revealed (Can take ± values). This section also shows when to quickly drain the oil into the reserve tank (-CST: means drain the tank quickly, 0: means continue using the current CST value) in off-road driving mode (Output 2). Based on this data, instant changes can be made to existing shock absorbers.

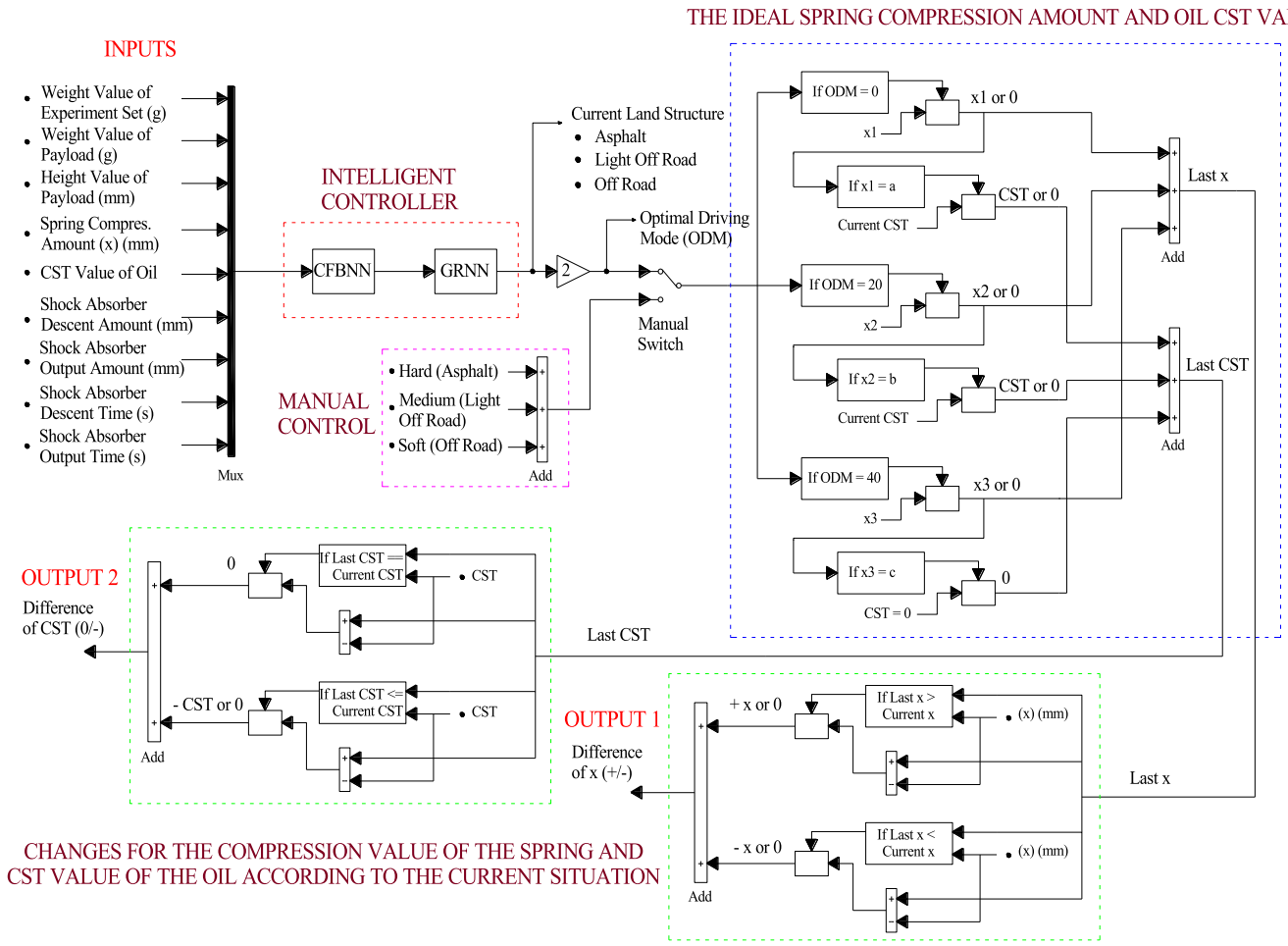


Fig. 10. System control block (Automatic and manual control).

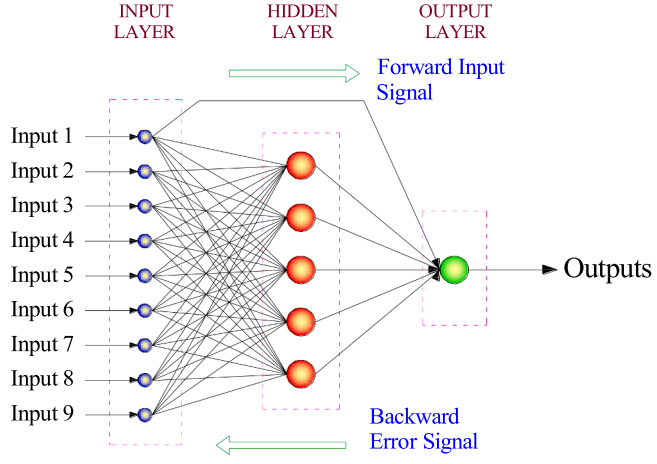


Fig. 11. CFBNN network structure.

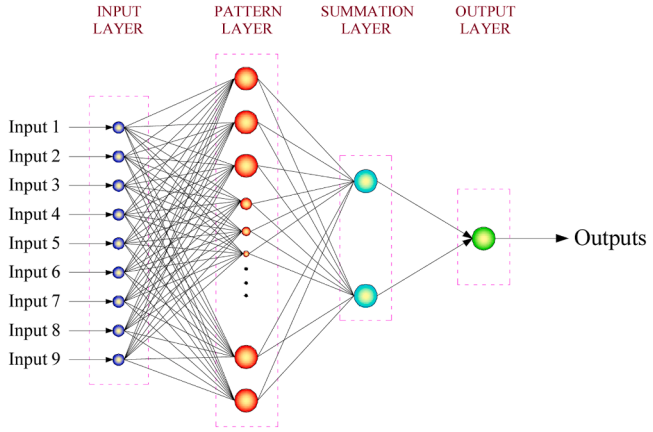
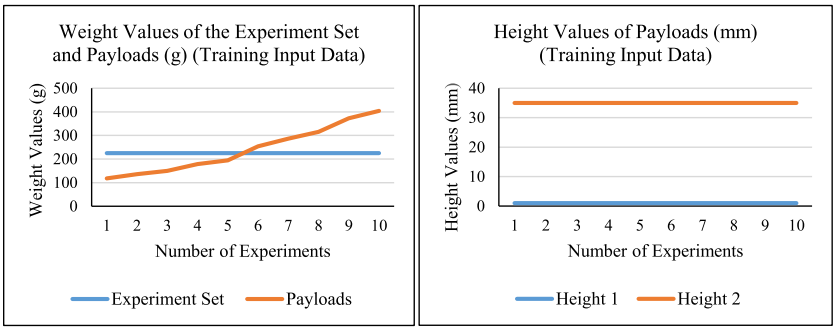


Fig. 12. GRNN network structure.

2.2.2. *Cascade forward-back propagation neural networks (CFBNN)*

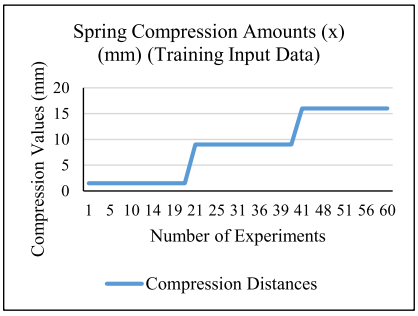
Cascade-forward networks resemble feed-forward networks but differ by incorporating connections from the input and all preceding layers to each subsequent layer. Similar to feed-forward networks, cascade networks with two or more layers are capable of approximating any finite input-output mapping with arbitrary accuracy, provided a sufficient number of hidden neurons [28]. Studies on multilayer feed-forward networks can be traced back to the pioneering work of Rosenblatt (1962) and Widrow (1962). The backpropagation algorithm provided a computationally efficient approach for training multilayer feedforward networks. The development and popularization of back-propagation as a practical method is commonly credited to Rumelhart et al. (1986) [29].

This network structure is used in many fields. Building credit scoring models in the credit union environment [29], alphabet recognition [30], industrial control [31], voice recognition [32], a programmable on-chip BP learning neural network study [33], birdsong recognition [34], signal and image processing [35]. The Neural Network Toolbox (>nntool) in MATLAB/Simulink was utilized for training these network

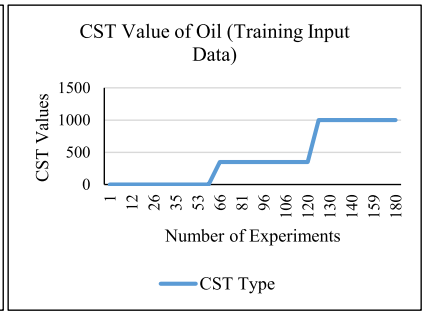


a) First and second input data.

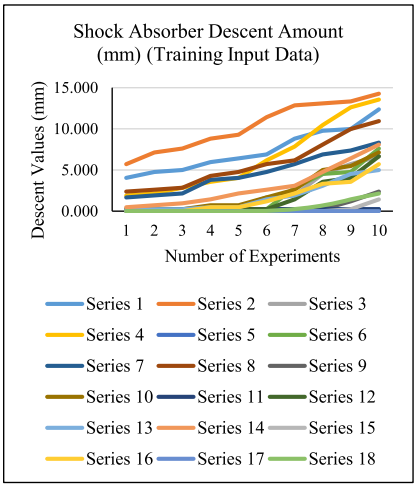
b) Third input data.



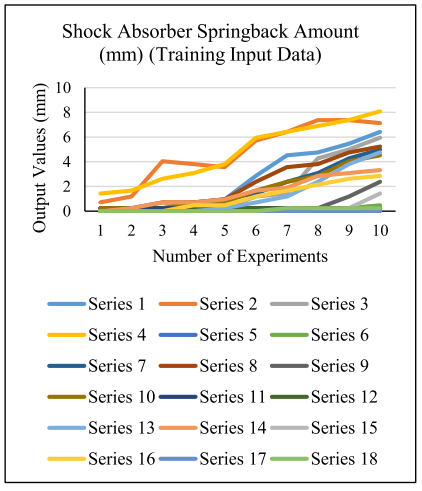
c) Fourth input data.



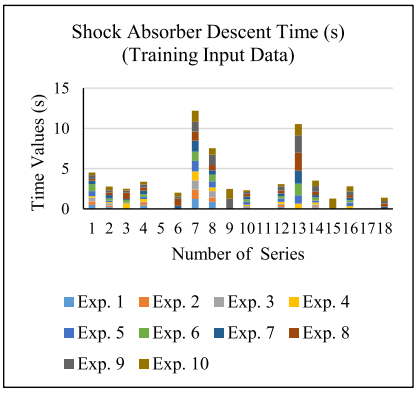
d) Fifth input data.



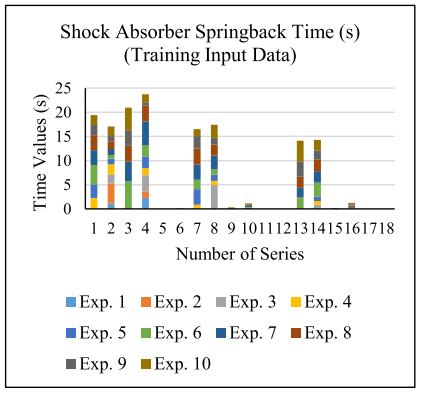
e) Sixth input data.



f) Seventh input data.



g) Eighth input data.



h) Ninth input data.

Fig. 13. Training input data.

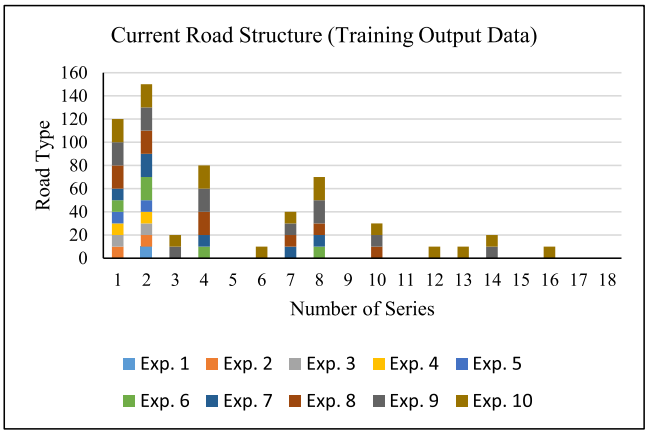


Fig. 14. Training output data.

architectures. Across all experiments, the number of epochs was 1000, the performance goal was 0, and the max_fail parameter was 10. In retraining, weights (W) or bias (b) values were not revised by hand. Fig. 11 shows a CFBNN network structure prepared for this study.

2.2.3. General regression neural network (GRNN)

The general regression neural network is a type of network architecture employed for system modeling and predictions based on varying parameters. Originally introduced by Donald F. Specht in 1991, it is founded on the Nadaraya-Watson Kernel Method (Kiyan and Yildirim, 2004). This network architecture features a rapid training process and performs effectively even with limited data. The GRNN architecture is a type of feedforward neural network that operates based on the probability density function. This network architecture consists of four distinct layers. The number of input neurons depends on the number of problem inputs, as in other networks. The number of neurons in the intermediate layer is equal to the number of samples. The number of neurons in the summation layer is one more than the number of outputs [36]. Today, the GRNN network structure is used in many fields. Some of those are: intelligent hybrid control method for gantry cranes [26,37], processor design for early screening of breast cancer [38], physical health evaluation by using a wearable smart bracelet system [39], renewable energies generation and carbon dioxide emission forecasting [40], signature recognition [41].

The *spread* value is selected by the user during the programming phase. The meaning of a broader *spread* is causing more space around the input vector. The smaller the number for the *spread* value means the better the best-fit approximation. The higher the value, the smoother the performance of the approximation (Sahroni, 2013). Fig. 12 shows a GRNN network structure prepared for this study.

3. Experiment studies

In this study, machine learning methods CFBNN and GRNN were preferred. Nine different types of input data were used, while one output data was obtained in CFBNN and GRNN.

On the other hand, one input data was used, while one output data was obtained in GRNN at the CFBNN+GRNN serial usage. Training input data and output data are shown, respectively, in Fig. 13 and Fig. 14. Also, testing input data and output data are shown, respectively, in Fig. 15 and Fig. 16. In these network structures, 180 rows of data were utilized as training data, and 72 rows of data were used as test data. During training data, ten different weight values were repeated eighteen times across ten lines of data. Two different height values were repeated nine times across twenty lines of data. Three different spring compression values were repeated three times across sixty lines of data. Three different oil CST values were repeated once across one hundred and eighty lines of data. During test data, nine different weight values were repeated eight times across nine lines of data. Two different height values were repeated four times across eighteen lines of data. Two different spring compression values were repeated twice across thirty-six lines of data. Two different oil CST values were repeated once across seventy-two lines of data.

The test data have not been previously presented to the networks. The success rates of the networks were interpreted with the results of R^2, RMSE, and MAE. Thus, it will have been tested how close artificial intelligence methods can get to the real experimental results with these error values. The success rates of the networks were determined by the fact that the R^2 results were close to 1, while the RMSE and MAE results were near 0.

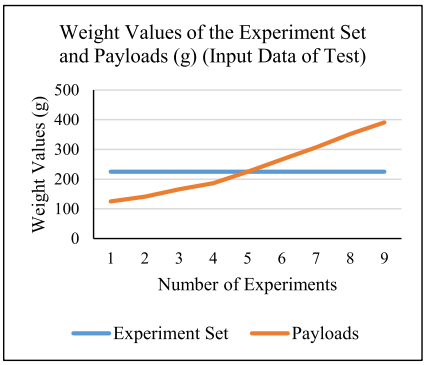
4. Results

4.1. GRNN experiment results

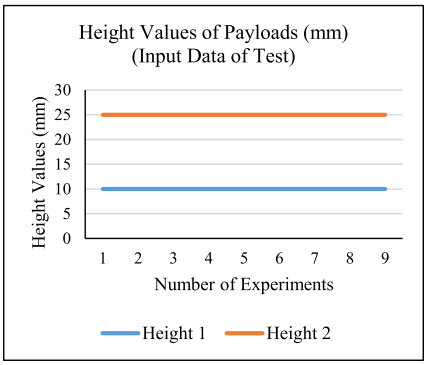
This study tested nine different *spread* values (0.000001, 0.00001, 0.0001, 0.001, 0.01, 0.1, 1, 10, and 100) to determine the optimal performance. As represented in Table 1, it can be observed that the training and test results remain unchanged for values where the *spread* value is 0.1 or lower, up to four decimal places. The 'Train $R^{2\prime}$ result is one, the 'Train RMSE' result is zero, and the 'Train MAE' result is zero at the first six *spread* values. But the optimal performance was determined with a *spread* value of 1. Because, especially when comparing networks with a spread value of 0.1 and 1, the network with a spread value of 1 has lower error results and higher success rates.

When examining the success rates of the nine different networks in Table 2, all success rates for the first six networks remain the same, while the error success rates for the other networks begin to decrease. Standard deviation is a measure of central dispersion. It indicates how far, on average, the values in a data set deviate from the mean. A small standard deviation indicates that the values are not very far from the mean, while a large standard deviation indicates that they are. A small standard deviation indicates a non-uniform distribution; the opposite indicates a dispersed distribution. If all values in the data set are equal, the standard deviation equals zero. The standard deviation results for the networks are shown in the last two rows of Table 2. The values did not deviate very far from the mean. The results for the first six networks are identical. For the last three networks, the standard deviation values of the networks decrease, but the percentage success rates also decrease. Meanwhile, Table 3 shows the average error values of cross-validation in GRNN. Here, the network with a *spread* value of 1 has better success rates than the network with a *spread* value of 0.1.

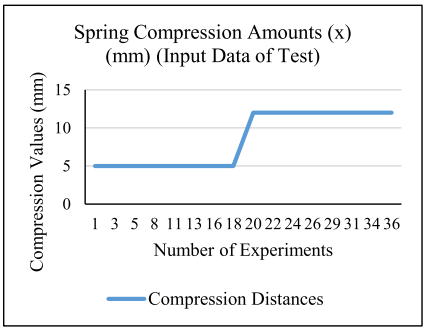
To measure how well the training success is, the cross-validation method was applied to the networks in this study. Here, the original dataset was split into two. 180 rows of data (71.43 %) were used as training data, and 72 rows of data (28.57 %) were used as test data. The training set was divided into three equal parts (3-fold). Also, there is one part to test (1-fold). A total of four data sets (4-fold) were used, and their different results were obtained from the tests, and their averages were calculated. Thus, the validated training error results were found. The results are shown in Table 4 for only *spread* 1 in GRNN. Here, the average result values are more reliable for evaluating the success of the network. Here, appropriate learning has occurred rather than excessive or inadequate learning. In most cases, if the data set is small, randomly splitting such data may not be a good idea. The results it was found using only training and testing may not represent the true capability of the model. Instead, the data set is divided into n equal parts, and training and testing are performed separately. In this way, the performance of the model on data it does not see can be measured more reliably. Therefore, cross-validation is crucial for model validation. As the data set grows, the characteristics are largely preserved. For example, if you use 200 data points out of 1 million for testing. Therefore, C.V. is not necessary for large datasets.



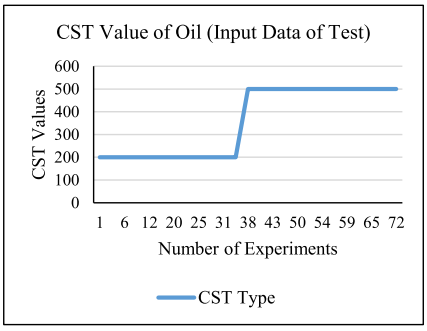
a) First and second input data.



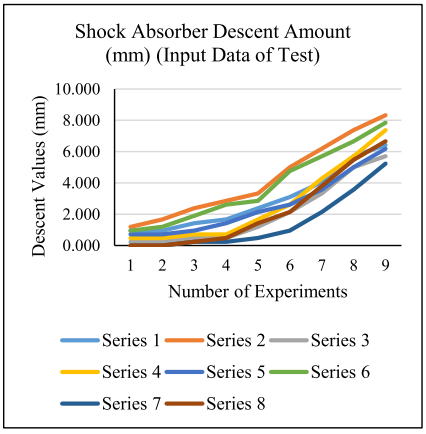
b) Third input data.



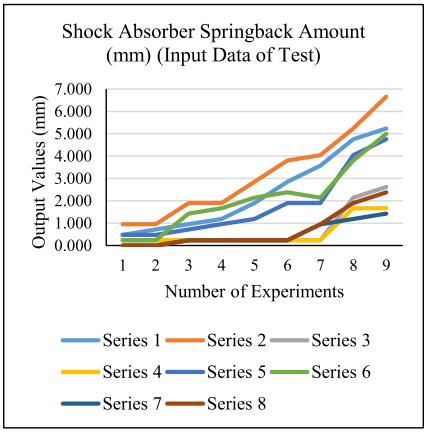
c) Fourth input data.



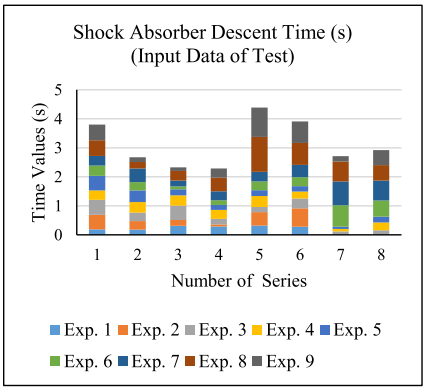
d) Fifth input data.



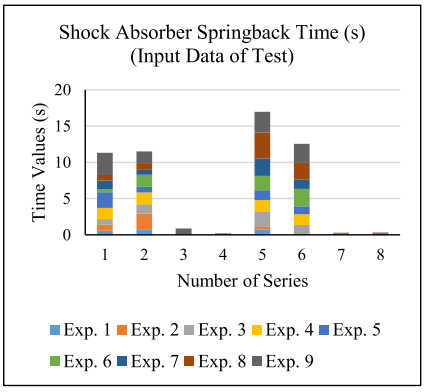
e) Sixth input data.



f) Seventh input data.



g) Eighth input data.



h) Ninth input data.

Fig. 15. Testing input data.

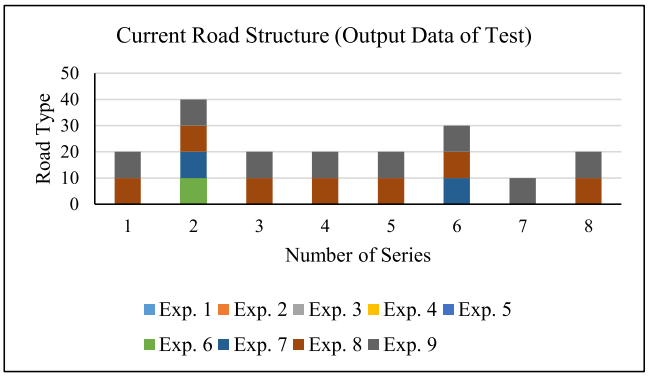


Fig. 16. Testing output data.

4.2. CFBNN experiment results

Table 5 shows the training data features of the CFBNN network. The training function is Trainbfg. The learning function (Adaption Learning Function) is Learngdm, the number of hidden layer neurons is 5, the transfer function used in the hidden layer neurons is Logsig, the number of neurons used in the output layer is 1, and the transfer function in this layer is Purelin. Table 6 shows the training results of this network, too. The results shown in the first row are the results calculated in the Excel program. The test results are the results of data that has never been introduced to the network before.

The second row results are the values obtained as a result of training in the nntool toolbox in Simulink and can be seen in Fig. 17, too. During training, the toolbox randomly selects the data required for training, validation, and testing from the total data. Fig. 17 shows the training performance graphs of the CFBNN network. Fig. 17a shows the training performance, Fig. 17b shows the training state, and Fig. 17c shows the training regression. The last row (Third row) shows the standard deviation values of the network. The values did not deviate very far from the mean.

Table 4
Cross-validation percentage success values for GRNN (*Spread*=1) (4-fold C.V.).

Errors	Split 1	Split 2	Split 3	Split 4	Mean Values
Train Data for 5 %	100 %	83.33 %	78.33 %	100 %	90.42 %
Test Data for 5 %	65.28 %	58.33 %	68.06 %	80.56 %	68.06 %
Train Data for 10 %	100 %	83.33 %	78.33 %	100 %	90.42 %
Test Data for 10 %	65.28 %	58.33 %	68.06 %	81.94 %	68.40 %

4.3. CFBNN+GRNN experiment results

This study tested nine different *spread* values (0.000001, 0.00001, 0.0001, 0.001, 0.01, 0.1, 1, 10, and 100) to determine the optimal performance. As represented in Table 7, it can be observed that the training and test results remain unchanged for values where the *spread* value is 0.001 or lower, up to four decimal places. The 'Train $R^{2'}$ result is one, the 'Train RMSE' result is zero, and the 'Train MAE' result is zero at the first four *spread* values. Therefore, the optimal performance was preferred with a *spread* value of 0.0001.

When examining the success rates of the nine different networks in Table 8, all success rates for the first four networks remain the same, while the error success rates for the other networks begin to decrease. The standard deviation results for the networks are shown in the last two rows of Table 8. The values did not deviate very far from the mean. The results for the first four networks are identical. For the last five networks, the standard deviation values of the networks decrease, but the percentage success rates also decrease. Meanwhile, Table 9 shows the average error values of cross-validation in GRNN in CFBNN+GRNN. While the success rates are the same in the first five network structures, the success rates decrease in the other networks.

The validated training error results are shown in Table 10 for only *spread* 1.10^{-4} in GRNN in CFBNN+GRNN. The average result values are

Table 1
The performance results of the *spread* values for GRNN.

Spread	1.10^{-6}	1.10^{-5}	1.10^{-4}	1.10^{-3}	1.10^{-2}	1.10^{-1}	1	10	100
Train.R^2	1	1	1	1	1	1	**1**	0.8753	0.3855
Test.R^2	0.4848	0.4848	0.4848	0.4848	0.4848	0.4848	**0.5350**	0.6143	0.6586
Trn.RMSE	0	0	0	0	0	0	**2.7E-18**	2.2811	4.7609
Test.RMSE	4.0824	4.0824	4.0824	4.0824	4.0824	4.0824	**3.5501**	2.7041	2.9445
Train.MAE	0	0	0	0	0	0	**2.0E-19**	1.4107	3.2689
Test.MAE	1.6666	1.6666	1.6666	1.6666	1.6666	1.6666	**1.4588**	1.5877	2.4333

Table 2
Percent success rates of the networks for 5 % and 10 % error values and standard deviations of the networks (GRNN).

Spread	1.10^{-6}	1.10^{-5}	1.10^{-4}	1.10^{-3}	1.10^{-2}	1.10^{-1}	1	10	100
5 % Train.	100 %	100 %	100 %	100 %	100 %	100 %	**100 %**	47.78 %	13.89 %
5 % Test.	83.33 %	83.33 %	83.33 %	83.33 %	83.33 %	83.33 %	**80.56 %**	47.22 %	0 %
10 % Train.	100 %	100 %	100 %	100 %	100 %	100 %	**100 %**	52.78 %	18.33 %
10 % Test.	83.33 %	83.33 %	83.33 %	83.33 %	83.33 %	83.33 %	**81.94 %**	52.78 %	0 %
Stn.D Train	6.0236	6.0236	6.0236	6.0236	6.0236	6.0236	**6.0236**	4.7955	3.0514
Stn.D. Test.	5.5664	5.5664	5.5664	5.5664	5.5664	5.5664	**5.0743**	3.7018	2.0362

Table 3
Average values for cross-validation in GRNN (4-fold C.V.).

Spread	1.10^{-6}	1.10^{-5}	1.10^{-4}	1.10^{-3}	1.10^{-2}	1.10^{-1}	1	10	100
Train.R^2	1	1	1	1	1	1	**1**	0.8794	0.4458
Test.R^2	0.3377	0.3377	0.3377	0.3377	0.3377	0.3377	**0.3502**	0.3612	0.3530
Trn.RMSE	0	0	0	0	0	0	**1.2E-17**	2.0329	4.2721
Test.RMSE	4.8792	4.8792	4.8792	4.8792	4.8792	4.8792	**4.7461**	4.5950	4.2985
Train.MAE	0	0	0	0	0	0	**9.7E-19**	1.1422	2.9581
Test.MAE	2.4305	2.4305	2.4305	2.4305	2.4305	2.4305	**2.3786**	2.5769	3.0310

Table 5
CFBNN training features.

Network Type	Training Function	Ad. Learn. Function	Hidden Layer Neurons	H. Layer Trans.Fun.	Output Layer Neurons	O. Layer Trans.Fun.
CFBNN	Trainbfg	Learngdm	5	LOGSIG	1	PURELIN

Table 6
CFBNN training results.

Train. R^2	Test R^2	Train. RMSE	Test RMSE	Train. MAE	Test MAE
0.9089	0.7706	1.8131	2.1323	1.2674	1.6695
Best V. Perf.	**Gradient**	**Train. R**	**Valid. R**	**Test R**	**All R**
1.4904	1.5154	0.9456	0.9801	0.96832	0.95339
		Stn.D. Train	**Stn.D. Test**		
		5.7403	3.8881		

more reliable for evaluating the success of the network. Here, appropriate learning has occurred. No overfitting occurred here. In this model, results were obtained on the test data that were approximately as good as those on the training data.

4.4. Comparison of experiment results

In the present study, two distinct artificial intelligence techniques from machine learning methods were used. As shown in Table 11, the CFBNN+GRNN method produced the best results. In the 5 % error rate evaluation, 100 % success was attained in the training data, and 98.96 % success was attained in the test data. The success rates of GRNN and CFBNN networks were lower than those of serial use, even in the 10 % error rate evaluations. No cross-validation was performed for CFBNN, which ranked third, because the 5 % and 10 % error evaluation results were below 12 %.

5. Results and discussions

In the current study, while creating the model, real-time measurement values obtained from experimental studies were taken into account

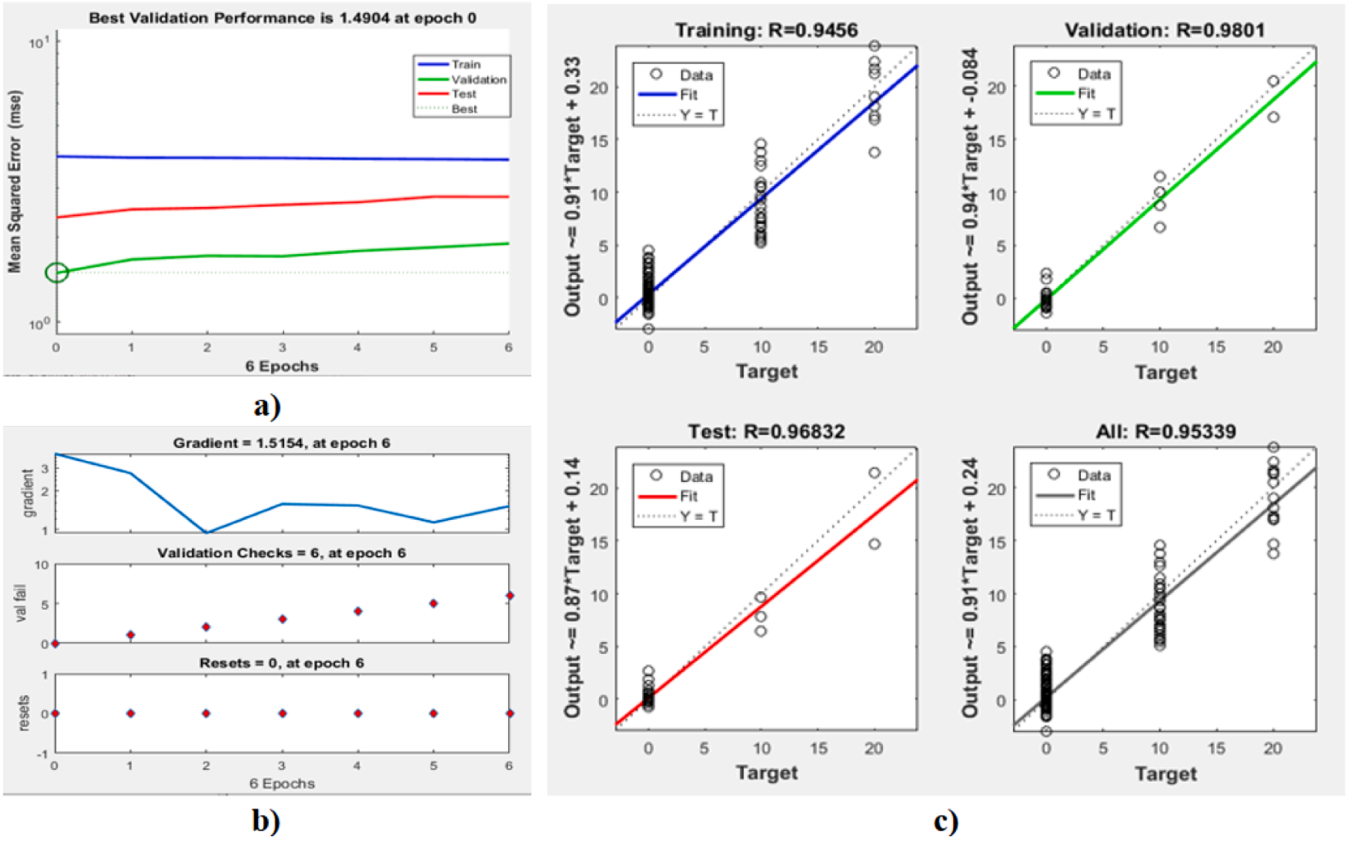


Fig. 17. CFBNN training performance graphs: a) Training performance, b) Training state, c) Training regression.

Table 7
The performance results of *spread* values for GRNN in CFBNN+GRNN.

Spread	1.10^{-6}	1.10^{-5}	1.10^{-4}	1.10^{-3}	1.10^{-2}	1.10^{-1}	1	10	100
Train.R^2	1	1	**1**	1	0.9940	0.9900	0.9793	0.8239	0.9086
Test.R^2	1	1	**1**	1	1	0.9952	0.9482	0.7472	0.7709
Trn.RMSE	0	0	**0**	2.2E-11	0.4625	0.5984	0.8639	4.0168	5.9822
Test.RMSE	0	0	**0**	0	6.4E-47	0.3020	0.9884	3.5840	4.3617
Train.MAE	0	0	**0**	2.3E-12	0.0487	0.0854	0.2059	2.8749	4.7539
Test.MAE	0	0	**0**	0	7.6E-48	0.0355	0.2925	2.7146	4.0558

Table 8
Percent success rates of the networks for 5 % and 10 % error values and standard deviations of the networks (GRNN in CFBNN+GRNN).

Spread	1.10^{-6}	1.10^{-5}	1.10^{-4}	1.10^{-3}	1.10^{-2}	1.10^{-1}	1	10	100
5 % Train.	100 %	100 %	**100 %**	100 %	98.88 %	97.77 %	90 %	0 %	0 %
5 % Test.	100 %	100 %	**100 %**	100 %	100 %	98.61 %	84.72 %	0 %	0 %
10 % Train.	100 %	100 %	**100 %**	100 %	98.88 %	97.77 %	91.66 %	0 %	0 %
10 % Test.	100 %	100 %	**100 %**	100 %	100 %	98.61 %	84.72 %	0 %	0 %
Stn.D Train	6.0236	6.0236	**6.0236**	6.0236	6.0008	5.9820	5.9137	2.4191	0.0260
Stn.D. Test.	4.3605	4.3605	**4.3605**	4.3605	4.3605	4.3502	4.2468	0.9721	0.0175

Table 9
Average values for cross-validation in GRNN in CFBNN+GRNN (4-fold C.V.).

Spread	1.10^{-6}	1.10^{-5}	1.10^{-4}	1.10^{-3}	1.10^{-2}	1.10^{-1}	1	10	100
Train.R^2	1	1	**1**	1	0.9971	0.9941	0.9716	0.8219	0.8757
Test.R^2	0.9735	0.9735	**0.9735**	0.9735	0.9735	0.9723	0.9659	0.8112	0.8267
Trn.RMSE	0	0	**0**	1.1E-11	0.2312	0.4149	0.9263	3.9727	5.5346
Test.RMSE	0.7112	0.7112	**0.7112**	0.7112	0.7112	0.7868	0.9198	4.0945	5.4058
Train.MAE	0	0	**0**	1.1E-12	0.0243	0.0606	0.2562	2.9617	4.4831
Test.MAE	0.1041	0.1041	**0.1041**	0.1041	0.1041	0.1132	0.2489	3.1306	4.5793

Table 10
Cross-validation percentage success values for GRNN in CFBNN+GRNN (*Spread*=1.10^{-4}) (4-fold C.V.).

Errors	Split 1	Split 2	Split 3	Split 4	Mean Values
Train Data for 5 %	100 %	100 %	100 %	100 %	100 %
Test Data for 5 %	97.22 %	98.61 %	100 %	100 %	98.96 %
Train Data for 10 %	100 %	100 %	100 %	100 %	100 %
Test Data for 10 %	97.22 %	98.61 %	100 %	100 %	98.96 %

instead of the mathematical model of the classical control algorithm, Skyhook. Artificial intelligence methods were used to analyze instant road conditions using nine different types of data. These data are respectively: 1- Weight Value of Experiment Set (g), 2- Weight Value of Payload (g), 3- Height Value of Payload (mm), 4- Spring Compression Amount (x) (mm), 5- CST Value of Oil, 6- Shock Absorber Descent Amount (mm), 7- Shock Absorber Springback Amount (mm), 8- Shock Absorber Descent Time (s), and 9- Shock Absorber Springback Time. (s). This input data diversity can be further increased in tests to be performed on motorcycles. By adding different sensors to the system, issues such as the motorcycle's cornering ability, driving stability on sloping terrain, sensitivity to speed, grip skills on snowy and wet roads, chassis stability, air pressure and temperatures, driver safety during sudden braking and sudden starts, and compatibility with the traction control system can be addressed. Thanks to all this data, both vehicle safety and driver safety can be increased to a higher level by making general changes in the system with artificial intelligence methods. The road conditions where motorcycles are used are constantly changing. Especially in off-road driving, steep ups and downs, jumps, jumping over potholes, difficulties in holding on to the road due to variable weather conditions in asphalt driving, and the presence of possible stones and potholes on light off-road roads require shock absorbers to adapt to nonlinear situations. Apart from these, the constant change of the lean angle of the motorcycle on bends, the different damping rates of each shock absorber for safety purposes in sudden movements, and the increase in shock absorber hardness at high speeds, all increase the complexity of the driving safety issue. After all, every motorcyclist has a different weight. Also, the addition of a second person to the motorcycle and the loads, items, and luggage bags added to the motorcycle cause the system dynamics to change again, and the security measures to be reconsidered. All these variables make it necessary to use artificial intelligence methods in system designs for safe driving. In the current study, CFBNN and GRNN artificial neural networks from machine learning methods were used in a serially connected manner. According to the available data, the current road situation could be predicted with a 98.96 % success rate. The current study can guide the design of safer driving systems.

6. Conclusion

When previous studies are examined, the use of artificial intelligence in shock absorbers is mostly encountered in soft sensor design [9–11,13,14]. It is anticipated that the use of technologies such as visual processing or lidar sensors on motorcycles as an alternative to determining road conditions according to existing shock absorber responses may lead to earlier detection of potential safety problems.

CRediT authorship contribution statement

Serkan Beller: Writing – review & editing, Writing – original draft, Visualization, Validation, Supervision, Software, Resources, Project administration, Investigation, Funding acquisition.

Table 11
Comparison of NNs according to cross-validation results.

	Network Type	Train Data for 5 % and 10 % Error	Test Data for 5 % and 10 % Error	Train R^2	Test R^2	Train RMSE	Test RMSE	Train MAE	Test MAE
1	**CFBNN**	**100 %**	**98.96 %**	**1**	**0.9735**	**0**	**0.7112**	**0**	**0.1041**
	+GRNN	**100 %**	**98.96 %**						
	Network Type	**Train Data for 5 % and 10 % Error**	**Test Data for 5 % and 10 % Error**	**Train R^2**	**Test R^2**	**Train RMSE**	**Test RMSE**	**Train MAE**	**Test MAE**
2	GRNN	90.42 %	68.06 %	1	0.3502	1.2E-17	4.7461	9.7E-19	2.3786
		90.42 %	68.40 %						
	Network Type	**Train Data for 5 % and 10 % Error**	**Test Data for 5 % and 10 % Error**	**Train R^2**	**Test R^2**	**Train RMSE**	**Test RMSE**	**Train MAE**	**Test MAE**
3	CFBNN	6.11 %	5.56 %	0.9089	0.7706	1.8131	2.1323	1.2674	1.6695
	(Not C.V.)	12.22 %	9.72 %						

Declaration of competing interest

The authors declare that they have no known competing financial interests or personal relationships that could have appeared to influence the work reported in this paper.

Acknowledgments

The Scientific Research Projects Unit of Çukurova University supported the present work. Project code: FBA-2023–16425

Data availability

No data was used for the research described in the article.

References

[1] https://www.tiryakilerlastik.com/blog/icerik/suspansiyon-nedir (Accessed date: 01.06.2025).
[2] https://www.servispasaoglu.com.tr/blog/suspansiyon-nedir (Accessed date: 01.06.2025).
[3] https://www.motorcular.com/tr/moto-teknik/motosiklette-suspansiyon-1 (Accessed date: 01.06.2025).
[4] C.F. Nicolas, J. Landaluze, E. Castrillo, M. Gaston, R. Reyero, Application of fuzzy logic control to the design of semi-active suspension systems, in: *Proceedings of 6th International Fuzzy Systems Conference* Barcelona Spain (2), 1997, pp. 987–993, https://doi.org/10.1109/FUZZY.1997.622843.
[5] L. Wu, W. Ren, K. Ba, X. Wang, J. Zhang, X. Kong, B. Yu, Control algorithm design of motorcycle semi-active suspension system via frequency division, J. Mech. Sci. Technol. 38 (1) (2024) 33–47, https://doi.org/10.1007/s12206-023-1204-0.
[6] W.E. Misselhorn, N.J. Theron, P.S. Els, Investigation of hardware-in-the-loop for use in suspension development, Veh. Syst. Dyn. 44 (1) (2006) 65–81, https://doi.org/10.1080/00423110500303900.
[7] A.J. Qazi, A. Khan, M.T. Khan, S. Noor, A parametric study on performance of semi-active suspension system with variable damping coefficient limit, in: 2013 AASRI Conference on Intelligent Systems and Control AASRI Procedia 4, 2013, pp. 154–159, https://doi.org/10.1016/j.aasri.2013.10.024.
[8] M. Garziad, A. Saka, Modelling and control of a semi-active suspension system of motorcycle, modelling and control of a semi-active suspension system of motorcycle, in: 2018 International Conference on Electronics, Control, Optimization and Computer Science (ICECOCS), Kenitra Morocco, 2018, pp. 1–8, https://doi.org/10.1109/ICECOCS.2018.8610635.
[9] D. Capriglione, M. Carratù, A. Pietrosanto, P. Sommella, Soft sensors for instrument fault accommodation in semiactive motorcycle suspension systems, IEEe Trans. Instrum. Meas. 69 (5) (2020) 2367–2376.
[10] D. Capriglione, M. Carratù, C. Liguori, V. Paciello, P. Sommella, A soft stroke sensor for motorcycle rear suspension, Measurement 106 (2017) 46–52.
[11] M. Carratù, A. Pietrosanto, P. Sommella, V. Paciello, Measuring suspension velocity from acceleration integration. Proc. IEEE Int. Workshop Metrology for Automotive (MetroAutomotive), 2018, pp. 933–938, https://doi.org/10.1109/MetroAuto.2018.8486919.
[12] D. Delvecchio, C. Spelta, G. Perico, S.M. Savaresi, Accelerometer-based estimation of the elongation speed in a motorcycle suspension via Kalman-Filter techniques, in: 49th IEEE Conference on Decision and Control, Hilton Atlanta Hotel Atlanta GA USA 978-1-4244-7746-3/10/$26.00 ©2010 IEEE 5566-5571, 2010.
[13] A. Beghi, M. Liberati, S. Mezzalira, S. Peron, Grey-box modeling of a motorcycle shock absorber for virtual prototyping applications, Simul. Model. Pract. Theory. 15 (2007) 894–907.
[14] D. Capriglione, M. Carratù, A. Pietrosanto, P. Sommella, NARX ANN-based instrument fault detection in motorcycle, Measurement 117 (2018) 304–311.
[15] M.E. Emekli, Hafif ticari bir araç için yarı aktif süspansiyon sistemi tasarımı. Mechatronics Engineering, İstanbul Technical University Master's Thesis, 2008, p. 118.
[16] P.S. Çetinkaya, Taşıt Mekaniği, 9th Edition, Nobel Akademik Yayıncılık, 2023, p. 458. April.
[17] https://www.cycleworld.com/sport-rider/tech/semi-active-suspension/(Accessed date: 04.06.2025).
[18] https://polen.itu.edu.tr/items/2cb9ea84-fc8e-4eeb-8ed3-ed406f0aad24 (Accessed date: 04.06.2025).
[19] https://bike-test.com/en/mtb-tech/rear-shocks-with-piggyback/ (Accessed date: 06.06.2025).
[20] https://www.shocksurplus.com/blogs/shocks-101/shock-absorber-designs-emulsion-foam-cell-nitrogen-gas-monotube-reservoir (Accessed date: 06.06.2025).
[21] https://www.turkrc.com/rc-amortisor-yagi-degisimi/(Accessed date: 07.08.2025).
[22] https://www.kalyoncumotor.com/blog/icerik/motosiklet-yaglarinin-cesitleri-ve-ozellikleri (Accessed date: 07.08.2025).
[23] https://motoiservices.com/en/suspension-oil-equivalence-chart/ (Accessed date: 07.08.2025).
[24] https://ohlins.pl/sites/default/files/reclist_2017_web.pdf (Accessed date: 07.08.2025).
[25] https://www.motospartan.com.tr/blog-detay/motosiklet-amortisor-yagi-ne-zaman-degisir-110?srsltid=AfmBOoquNB0YGTZI0uv2-_5srj4IE74y6xfGZ4jDsr5vl4DJmx-O5Bqg (Accessed date: 07.08.2025).
[26] H. Yavuz, S. Beller, An intelligent serial connected hybrid control method for gantry cranes, Mech. Syst. Signal. Process. 146 (2021) 107011, https://doi.org/10.1016/j.ymssp.2020.107011.
[27] S. Beller, Torque estimation with artificial intelligence methods in a brushed geared DC motor, Çukurova Univ. J. Fac. Eng. 37 (4) (2022) 885–898, https://doi.org/10.21605/cukurovaumfd.1230790.
[28] https://www.mathworks.com/help/deeplearning/ref/cascadeforwardnet.html?s_tid=srchtitle_cascadeforwardnet_1 (Accessed date: 10.09.2021).
[29] V.S. Desai, J.N. Crook, G.A. Overstreet Jr, A comparison of neural networks and linear scoring models in the credit union environment, Eur. J. Oper. Res. 95 (1996) 24–37.
[30] S.B. Yun, Y.J. Kim, S.S. Dong, C.H. Lee, Hardware implementation of neural network with expansible and reconfigurable architecture, in: 9th International Conference on Neural Information Processing 2, 2002, pp. 970–975.
[31] H. Wegmann, Fuzzy control and neural networks industrial applications in the world of PLCs, in: Conference on Control Applications II, IEEE Piscataway, 1994, pp. 1245–1249.
[32] T. Shima, T. Kimura, Y. Kamatani, T. Itakura, Y. Fujita, T. Iida, Neuro chips with on-chip back-propagation and/or hebbian learning, IEEe J. Solid-State Circuits. 27 (12) (1992) 1868–1876.
[33] C. Lu, B. Shi, L. Chen, A programmable on-chip BP learning neural network with enhanced neuron characteristics, in: IEEE International Symposium on Circuits and Systems 3, ISCAS, 2001.
[34] A. McIlraith, H. Card, Birdsong recognition with DSP and neural networks, in: Communications, Power, and Computing Conference Proceedings 2, IEEE, 1995.
[35] G. Leonhard, E. Cousin, J. Laisne, J. LeDrezen, G. Ouvradou, A. Maubant, A. Thepaut, Armenx: a flexible platform for signal and image processing, Proc. Soc. Photo-Opt. Instrum. Eng. (SPIE) 2607 (1995) 71–82.
[36] Ş. Sağıroğlu, E. Beşdok, M. Erler, Mühendislikte Yapay Zeka Uygulamaları I, Yapay Sinir Ağları, UFUK Yayıncılık, Kayseri, 2003.
[37] S. Beller, H. Yavuz, Crane automation and mechanical damping methods, Alex. Eng. J. 60 (2021) 3275–3293.
[38] W.H. Land Jr., X. Ma, E. Barnes, X. Qiao, J. Heine, T. Masters, J.W. Park, PNN/GRNN ensemble processor design for early screening of breast cancer, Procedia Comput. Sci. 12 (2012) 438–443.
[39] Y. Dai, J. Guo, L. Yang, W. You, A new approach of intelligent physical health evaluation based on GRNN and BPNN by using a wearable smart bracelet system, Procedia Comput. Sci. 147 (2019) 519–527.
[40] A. Heydari, D.A. Garcia, F. Keynia, F. Bisegna, L.D. Santoli, Renewable energies generation and carbon dioxide emission forecasting in microgrids and national grids using GRNN-GWO methodology, Energy Procedia 159 (2019) 154–159.
[41] L.Y. Fannas, A.Y.B. Sasi, Off-line signature recognition based on angle features and GRNN neural networks, World Acad. Sci. Eng. Technol. Int. J. Comput. Inf. Eng. 7 (10) (2013).